PERGAMON

Planetary and Space Science 49 (2001) 1137–1149

Planetary and Space Science

www.elsevier.com/locate/planspasci

Low-frequency limit of Jovian radio emissions and implications on source locations and Io plasma wake

Philippe Zarka[a,*], Julien Queinnec[a], Frank J. Crary[b]

[a] *Observatoire de Paris, Département de Recherche Spatiale (DESPA), CNRS URA-264, 5 Place Jules Janssen, 92195 Meudon Cedex, France*

[b] *Department of Astrophysical and Planetary Sciences (LASP), University of Colorado, Boulder, CO 80309-0392, USA*

Received 15 February 2000; received in revised form 11 October 2000; accepted 13 October 2000

Abstract

After deriving from Ulysses-URAP measurements the low-frequency limit of the Jovian hectometer emission spectrum (250 ± 50 kHz at the -20 dB level below the emission peak), and confirming the absence of Io's control on Jovian radio emission below ~ 1 MHz, we propose a single common explanation for these low-frequency limits: both are well explained by the quenching of the generation mechanism (the cyclotron-maser instability) where the ratio f_{pe}/f_{ce} reaches a critical value (about 0.14) along the source field lines. This occurs in the external part of Io's plasma torus for the hectometer component, and in Io's dense plasma wake discovered by Galileo for the Io-dependent (decameter) component. As a consequence, we infer new constraints on Jovian radio source locations, which are found to extend along the $L \approx 6$ field lines intersecting Io's wake (where the electron density is up to 10–20 times higher than in the average torus) for the Io-dependent decameter emission, and along $L \approx 7$–9 field lines (with apex at ≈ 7–11 R_J) for the hectometer emission. We also infer that the broadband kilometer (auroral) emission originates from $L > 10$ field lines, with apex well beyond 12 R_J, closing in the distant Jovian magnetosphere or opened to the solar wind. These results confirm and precise the source locations obtained from direction-finding studies with Ulysses. Finally, we discuss implications in terms of source extent and of the origin of the accelerated electrons responsible for the emissions, and we derive lower limits on the proton concentration in Io's plasma wake.

1. Introduction

Jupiter's low-frequency (LF) radio emissions were originally discovered through ground-based radioastronomical observations at decameter (DAM) wavelengths (Burke and Franklin, 1955), above the Earth's ionospheric LF cutoff about 5–15 MHz. It was later shown that part of the Jovian decameter radio emission is "controlled" by the satellite Io (Bigg, 1964). Io-controlled emissions are detected preferentially for two specific ranges of Io-Jupiter-observer angles (or "Io-phase"), about 90° and 240° when counted counterclockwise from Io's superior conjunction as viewed by the observer (see e.g., Fig. 7.15 of Carr et al., 1983, and Figs. 75 and 76 of Genova et al., 1989). With the advent of space radio observations in the 1970s, it was realized that Jovian LF radio emissions extended to the hectometer (HOM) and kilometer (KOM) wavelength ranges (Carr et al., 1983). While KOM and DAM components are clearly distinct according to both their spectra and dynamic spectra (i.e., intensity versus time and frequency), the situation is less clear for HOM and DAM components. The HOM spectrum appears to be the extent towards low frequencies of the DAM spectrum, but dynamic spectra reveal a "patchy" HOM morphology while DAM is rather organized in time–frequency "arcs". This difference may be attributed to the fact that the radio receivers onboard Voyager spacecraft, which discovered and performed the first extensive observations of HOM, had very different spectral characteristics below 1.3 MHz (HOM range) and above that frequency (up to the DAM range) (Warwick et al., 1977). More recently, the radio experiments onboard the Galileo and Cassini spacecraft recorded Jupiter's radio emissions over a broad spectral range, from KOM to DAM wavelengths, with a unique receiver (see e.g., Fig. 1). These observations suggest that HOM patches are the LF extent of Io-independent DAM emissions (see also Genova et al., 1987).

However, Io-DAM arcs were also found to extend towards low frequencies, down to about 1–2 MHz, i.e., overlapping

* Corresponding author. Tel.: +33-0-1-4507-7663; fax: +33-0-1-4507-2806.

E-mail address: philippe.zarka@obspm.fr (P. Zarka).

0032-0633/01/$ - see front matter
PII: S0032-0633(01)00021-6

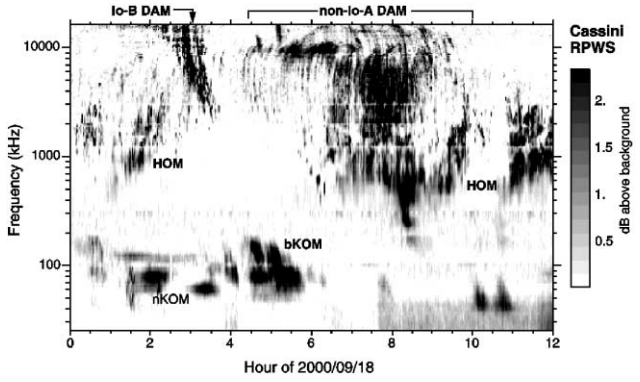

Fig. 1. Jovian LF radio emissions detected on 18 September 2000 by the RPWS (Radio and Plasma Waves Science) experiment onboard Cassini approaching Jupiter. The Io-controlled emission (labelled "Io-B DAM") appears here with a LF limit about 2 MHz, while Io-independent emission ("non-Io-A DAM") merges with the hectometer component ("HOM") detected down to 200–300 kHz. The auroral broadband kilometer component ("bKOM") is detected down to $\sim$ 40 kHz, while the narrowband emission ("nKOM") is certainly generated at or near f_{pe} in Io's torus.

with the HOM range (Carr et al., 1983). Early studies with the Radio Astronomy Explorer 1 satellite showed that Io's control was clearly visible down to 2.2 MHz but marginal at 1.3 MHz (Desch and Carr, 1978). This was better demonstrated by statistical studies of Voyager Planetary Radio Astronomy observations, in which Io's control is prominent at frequencies above $\sim$ 7 MHz but vanishes towards lower frequencies, being still present about 2 MHz but marginal or absent below $\approx$ 1 MHz (see Fig. 7 of Alexander et al., 1981). Dynamic spectra of LF Jovian radio emissions published in recent studies (Kaiser and Garcia, 1997; Lecacheux et al., 1998; Queinnec and Zarka, 1998) illustrate this fact, showing LF limits of Io-controlled DAM "arcs" about 2–3 MHz. This limit can be traced down to $\sim$ 1 MHz for some Io-controlled arcs visible in Voyager radioastronomy data (see e.g., about 0600 SCET in Fig. 1 of Ladreiter and Leblanc, 1991), and in Galileo radio observations (Menietti et al., 1998). Finally, our Fig. 1 displays a recent observation by the Radio and Plasma Waves Science experiment onboard Cassini (Gurnett et al., 2001) showing an Io-DAM arc with a typical LF limit about 2 MHz.

Io-controlled radio emissions presumably originate along Jovian magnetic field lines with shell parameter $L \approx 6$ (i.e., with apex at $\approx$ 6 Jovian radii from the planet's center in the frame of a dipolar field model), belonging to the instantaneous Io flux tube and/or crossing Io's Alfvènic wake. Along these field lines, the Io-Jupiter electrodynamic interaction is expected to accelerate electrons to keV energies (Crary and Bagenal, 1997; Queinnec and Zarka, 1998; and references therein), part of these accelerated electrons radiating then at the local electron gyrofrequency f_{ce}. The source of Io-independent DAM, more elusive, is thought to extend along $L > 6$ field lines (Genova et al., 1987). While it was understood very soon that the high-frequency limit of DAM emissions (controlled by or independent of Io), about 40 MHz, corresponds to the highest gyrofrequencies reached at or near the footprints of high latitude Jovian field lines (although a detailed agreement has not yet been obtained in the frame of the presently available magnetic field models (Connerney, 1992; Queinnec and Zarka, 1998)), the LF limit of Io's control has remained unexplained since its discovery some 20 years ago, as gyrofrequencies much lower than 1 MHz may be reached along the Io flux tube. This question has been often mentionned as an important scientific objective in recent projects of satellite radio monitoring of Jupiter (e.g., Zarka and Prangé, 1994).

One aim of this paper is to explain this LF limit about 1–2 MHz of the Io-controlled radio emission (that we will keep on calling "Io-DAM" even if it extends down to frequencies within the HOM range), in the light of recent Galileo spacecraft observations performed in Io's vicinity.

But Jupiter also possesses two other auroral radio components: the HOM and broadband kilometer (bKOM) emissions (there is a narrowband kilometer component—nKOM—, but it comes from within Io's torus). Using Ulysses radio observations (URAP experiment), some bKOM events have been shown to originate from $L = 9$–15 field lines (Ladreiter et al., 1994), while the HOM has been the subject of several studies with contrasted results: while some authors found a HOM source along $L \leqslant 6$ field lines (e.g., Reiner et al., 1993a), others found a range $L = 7$–11 (Ladreiter et al., 1994). Radio observations from Galileo by Kurth et al. (1997), as well as observations at other frequencies, favoured the latter range (see the discussion in Zarka, 1998). While bKOM was observed down to 20 kHz with Voyager (e.g., Ladreiter and Leblanc, 1989), and occasionally as low as 10–20 kHz in Ulysses-URAP observations (Kaiser et al., 1992), HOM was never observed below $\sim$ 60 kHz (Ladreiter and Leblanc, 1989), and is uncommon or weak below $\sim$ 200 kHz (see below).

The second aim of this paper is thus to precisely determine and explain these LF limits, and especially that of HOM.

As remarked by Desch (1980), the observed frequency range of a radio component is one of the most important constraints on its source region (location in the magnetosphere and spatial extent). Existence of Io's control down to 1–2 MHz, for instance, proves that "Io-DAM" is generated along a large part of the Io flux tube (or nearby field lines), and not only close to the planetary surface. We propose thus below explanations for the LF limit of Io's control of the DAM component, and for the LF limits of HOM and bKOM components. We discuss the implications in terms of source location and extent, and of the origin of the accelerated electrons responsible for the emissions, and we derive constraints on the proton concentration in Io's vicinity.

In Section 2, we analyze Ulysses-URAP observations during the Jupiter flyby in order to give stronger statistical grounds to the above LF limits. Section 3 introduces our explanation for the physical origin of these LF limits. Section 5 discusses their detailed values in the frame of our

latest knowledge of the Jovian magnetic field and of Io's plasma environment, as presented in Section 4. Finally, the last section summarizes our results and discusses them in comparison to previous Jovian radio source locations.

The appendix compares the dipolar field lines used to express radio source locations in terms of magnetic L-shells, and field lines computed using the more realistic O6 model with a current sheet contribution (see below). In the latter case, the concept of L-shell is no more relevant for $L \geqslant 6$ due to the field line stretching caused by the current sheet. So, we will rather define field lines through their apex distance (in Jovian radii, 1 $R_J = 71\,400$ km), or more shortly refer to a field line with apex at n R_J as "n R_J field line".

2. Ulysses-URAP observations

2.1. LF limit of Io's control of DAM emission

For several months preceding the Ulysses-Jupiter flyby in February 1992 (Stone et al., 1992), Jovian LF radio emissions were observed continuously with a high signal-to-noise ratio, from a quasi-fixed vantage point close to the ecliptic, i.e., in a geometry comparable to that of ground-based observations. These data are well adapted to the search for Io's control at low frequencies, that we have performed at the highest frequencies of the Ulysses-URAP radioastronomy receiver: 740 and 940 kHz.

144 s-averaged intensity measurements have been used, covering continuously the 100-day period from 1991/09/23 to 1991/12/31 (closest approach to Jupiter occurred on 1992/02/08), largely dominated by Jovian HOM (or LF DAM) at 740 and 940 kHz. Fig. 2a displays the distribution of occurrence of the measurements at 940 kHz exceeding 3 standard deviations of the background noise fluctuations, versus Jovian longitude of the observer (CML) and Io's phase. The histograms of Fig. 2b and c are the corresponding cumulated distributions of activity in 5°-bins of CML and of Io phase, respectively. The activity appears clearly modulated by the Jovian rotation, but not at all controlled by Io (the fluctuations on Fig. 2c are consistent with a purely statistical origin). The same analysis, performed at 740 kHz gives identical results, confirming the absence of Io's control below $\sim$ 1 MHz.

2.2. LF limit of HOM emission

Fig. 3 displays the average spectrum of bKOM and HOM components, computed over the same 100-day period as above, over the high-frequency band of the Ulysses-URAP receiver (12 channels, approximately log-spaced between 52 and 940 kHz). Episodes of Jovian nKOM (narrowband kilometer emission from Io's torus (see e.g., Reiner et al., 1993b)) as well as Solar type III radio bursts—identified through both visual inspection and computer recognition (de Lassus and Lecacheux, 1997)—have been removed from the data before computing the spectrum. As expected (see e.g., Fig. 1 of Zarka, 1998), this average spectrum presents two humps, corresponding to bKOM at low frequencies and HOM at high frequencies.

A parabolic fit through the HOM average spectrum (dashed in Fig. 3) gives an average HOM LF cutoff about 230 kHz over the period studied. The instantaneous cutoff varies with time between $\sim$ 200 and 300 kHz (see e.g., Fig. 1). HOM may be detected occasionally at lower frequencies (Ladreiter and Leblanc, 1989), but its average

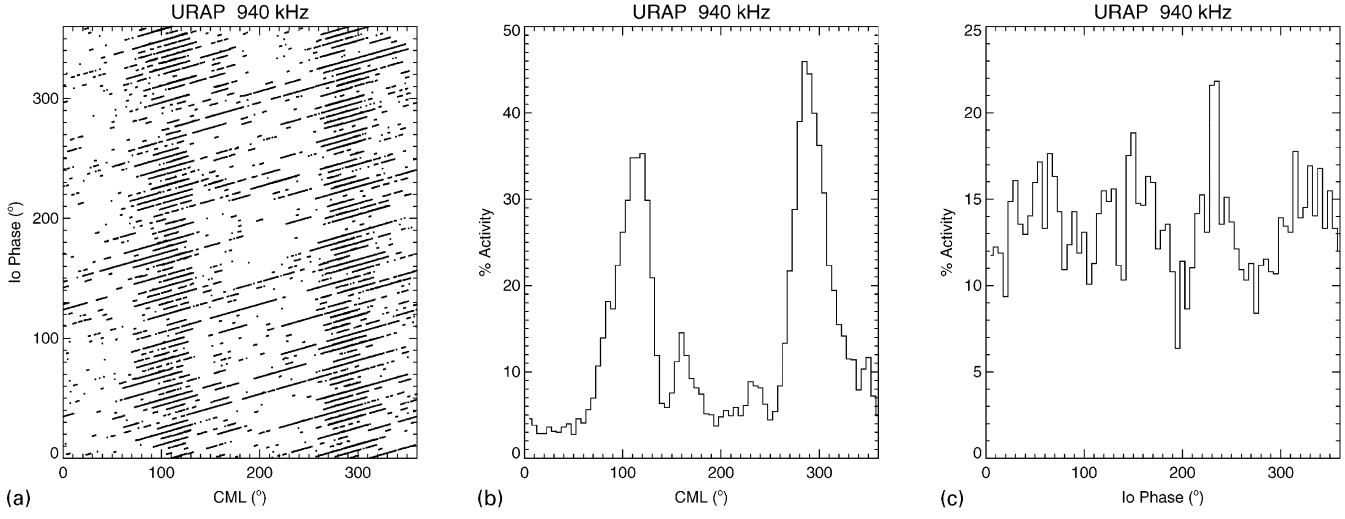

Fig. 2. (a) Distribution of occurrence of Ulysses-URAP 144 s-averaged intensity measurements exceeding 3 standard deviations of the background noise fluctuations, versus Jovian longitude of the observer (CML) and Io's phase. Data continuously cover a 100-day pre-encounter period (see text) dominated by Jovian HOM (or LF DAM) at 940 kHz. Histograms b and c are the corresponding cumulated distributions of activity at 940 kHz in 5°-bins of CML and of Io phase, respectively. Activity appears modulated by the Jovian rotation, not by Io's phase (the fluctuations in c are consistent with a statistical origin).

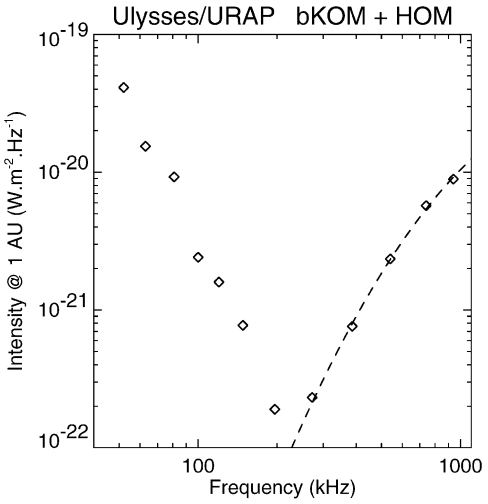

Fig. 3. Average spectrum of bKOM and HOM components, computed over the same 100-day period as Fig. 2, over Ulysses-URAP HF band. Jovian nKOM and Solar type III radio bursts have been removed from the data before computing the spectrum. The two humps of this average spectrum correspond to bKOM at low frequencies and HOM at high frequencies. A parabolic fit through the HOM spectrum (dashed) gives an average LF cutoff $\sim$ 230 kHz for the period studied.

power becomes negligible below $\sim$ 200 kHz, at least 20 dB below the bKOM level.

Similarly, bKOM may be detected occasionally up to $\sim$ 1 MHz, but with a negligible average contribution (see e.g., Boischot et al., 1981; Kaiser and Desch, 1992). Towards lower frequencies, bKOM can be detected down to 10–20 kHz in the LF range of the URAP receiver (and of Cassini-RPWS around the Jupiter flyby of December 2000).

3. Origin of low-frequency limits

It is now widely admitted that auroral planetary radio emissions are generated dominantly on the extraordinary (X) magneto-ionic mode through the so-called cyclotron-maser instability (CMI), first proposed for the auroral kilometric radiation of the Earth (AKR, also called "Terrestrial kilometric radiation"—TKR) by Wu and Lee (1979) (see the reviews by Louarn, 1992 and Zarka, 1998). Numerous subsequent observations and theoretical studies demonstrated that its efficient operation requires a very low ratio f_{pe}/f_{ce} in the source regions (see Benson, 1995; Hilgers, 1995; and references therein), f_{pe} being the electron plasma frequency ($f_{pe} \approx 9 \times N_e^{1/2}$, with f_{pe} in kHz and N_e in cm^{-3}) and f_{ce} the gyrofrequency ($f_{ce} \approx 2800 \times |\mathbf{B}|$, with f_{ce} in kHz and $|\mathbf{B}|$ in Gauss). This critical f_{pe}/f_{ce} CMI-quenching value was found to lie typically between $\sim$ 0.1 and 0.4. Of particular interest are the results of Hilgers (1992), who found an upper limit for AKR generation of $(f_{pe}/f_{ce})_{max} \approx 0.14$ from in situ Viking measurements during source crossings, and of Le Quéau et al. (1985) who predicted the existence of an efficiency threshold at $(f_{pe}/f_{ce})_{max} \approx 0.385$ from the study of wave growth and propagation in a realistic—inhomogeneous—auroral magnetic field.

Although one should be cautious when transposing these results to the generation of Jovian LF radio components (the magnetic field gradient length, proportional to the planetary radius, is $\sim$ 10 times larger at Jupiter than at Earth, leading to comparatively less inhomogeneous radio source regions; **B** and ∇**B** are less parallel in LF HOM and bKOM radio sources than in near-planetary auroral regions; hot electron velocity distributions may differ at the Earth and Jupiter; etc.), the requirement of a very low ratio f_{pe}/f_{ce} seems to be fulfilled in all auroral planetary radio sources (see Table 1 of Zarka, 1992a). We will thus consider below that the critical f_{pe}/f_{ce} CMI-quenching value lies between $\sim$ 0.14 and $\sim$ 0.4. In terms of the parameter $\varepsilon = (f_{pe}/f_{ce})^2$ used below, CMI operation and consequently X mode radio emission generation requires thus $\varepsilon \leqslant \varepsilon_{max}$, with $0.02 \leqslant \varepsilon_{max} \leqslant 0.15$.

In planetary magnetospheres other than the Jovian one, ε generally decreases with increasing distance (R) above the planetary surface because the magnetic field amplitude decreases approximately as a dipole, i.e., in R^{-3}, while the ionospheric electron density decreases exponentially. As a consequence, in these magnetospheres, the CMI-quenching value ε_{max} only fixes the high-frequency limit of the radio emission, while the LF limit is very low (a few kHz) and probably due to the vanishing plasma density in the magnetosphere a few radii away from the planet. At Jupiter, as noted by Crary (1998), the existence of Io's plasma torus considerably modifies this picture along field lines with apex between $\sim$ 5 and $\sim$ 10 R_J. ε only decreases in the ionosphere, up to $\sim$ 1.1 R_J from the planet's center, and then re-increases steadily with decreasing distance to the torus (see Fig. 4b). We suggest here that the LF limit of Io-controlled DAM, as well as that of the HOM spectrum, are due to the fact that the critical f_{pe}/f_{ce} CMI-quenching value ε_{max} is reached along the source field lines at low latitudes, in the torus vicinity, preventing radio emission at frequencies below $f_{ce}(\varepsilon_{max})$. We show below that this hypothesis is consistent with the available observations and deduce new constraints on Io-DAM, HOM and bKOM source regions.

4. Magneto-plasma observations and models

Present models of the Jovian magnetospheric plasma originating from Io and Io's torus are diffusive equilibrium models. The one by Bagenal (1994), valid between about 5 and 12 R_J relies on Voyager 1 near-equatorial observations in Io's torus. Assuming Maxwellian distributions, it extrapolates along Jovian magnetic field lines the plasma density and related parameters from the point where they have been measured. Moncuquet (1997) extended this model using Kappa distributions and Ulysses measurements across

Io's torus (along 7–9 R_J field lines) together with Voyager observations. Both models allow for a proton temperature anisotropy relative to the magnetic field direction, and lead to similar results as far as the total electron density is concerned, albeit with a larger latitudinal scale height above the centrifugal equator with the latter model. These models depend on the longitude only via the tilt between the centrifugal and magnetic equators (resp. tilted by $\sim 6.4^\circ$ and 9.6° with respect to the Jovigraphic equator).

Recent plasma density measurements in Io's torus by the Galileo spacecraft (Bagenal et al., 1997; Crary et al., 1998) suggested a density possibly twice as high as that measured by Voyager 1 outside Io's orbit, from ~ 6 to $8\,R_J$ (with a lower plasma temperature). These differences could also be due to torus density inhomogeneities localized in longitude or local time, which would indicate that the uncertainty affecting estimates of the average density profile across Io's torus can be as large as a factor ~ 2. Inside of $\sim 5\,R_J$ (cold torus), the density was found to decrease rapidly down to extremely low values, $\leqslant 3$ cm^{-3}. More important, Galileo's radio and plasma observations revealed a dense, extended cloud of plasma stagnating in Io's wake, with velocities $\leqslant 1$ km/s and a density up to $4\text{–}5 \times 10^4$ cm^{-3}, i.e., 10–20 times denser than the average torus (Gurnett et al., 1996; Frank et al., 1996; Louarn et al., 1997). Although we have no information on the characteristic time required to reach a diffusive equilibrium along field lines intersecting this dense plasma cloud, it is very likely that a permanent regime will be reached corresponding to an equatorial source much denser than the 2×10^3 cm^{-3} maximum density of the unperturbed torus. This assumption is supported by the interpretation by Gurnett et al. (1998) of a particular attenuation band in the HOM spectrum, which requires inhomogeneities of increased density along the Io L-shell.

In the present paper, we use for describing Io's torus the total electron density profiles derived from the Bagenal (1994) model. To describe the wake, we use an "upscaled" version of this model (including a scaling factor up to $\times 20$ on the equatorial measurements used as input parameters in the model), or compute diffusive equilibrium from Galileo measurements reported by Frank et al. (1996). Jupiter's ionospheric electron density is described using the recent model by Hinson et al. (1998), derived from a reanalysis of Voyager 2 occultation measurements: its vertical profile decreases with a ~ 900 km topside scale height above a maximum density layer of 3.5×10^5 cm^{-3} located 1600 km above the 1 bar level.

For Jupiter's internal magnetic field, we use the O6 model (Connerney, 1992), based on Voyager and Pioneer magnetometer measurements and also used in the above plasma models, and for comparison the recent VIP4 model (Connerney et al., 1998), including infrared observations of the Io flux tube footprint. In both cases, we include the Voyager current sheet model (hereafter CS) whose contribution to the Jovian magnetic field increases with the distance to the planet outside Io's orbit (Connerney et al., 1981). In the appendix, our results are converted into dipole L-shells (D4-offset tilted dipole-model by Smith et al., 1976) for comparison with Ulysses radio source location determinations.

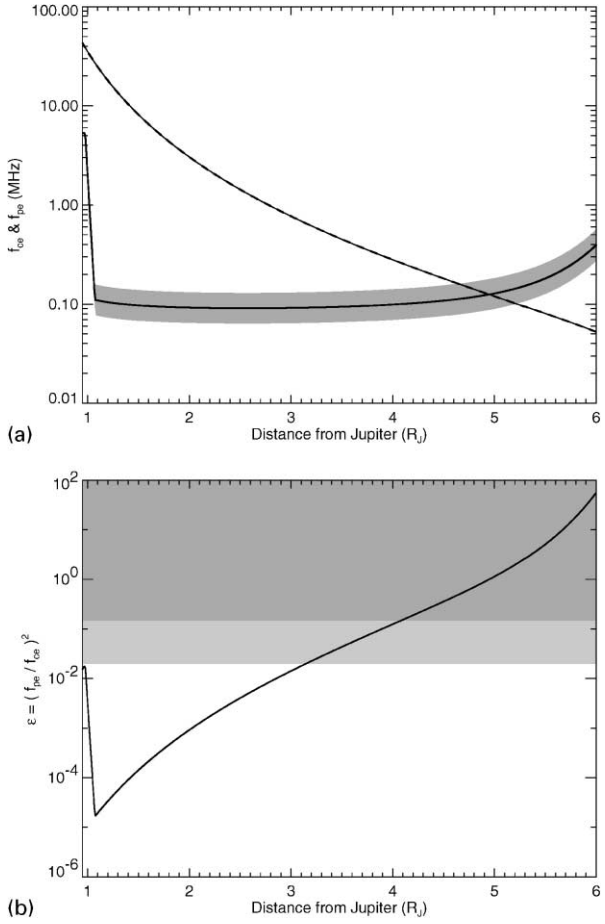

Fig. 4. (a) Variations of the local gyrofrequency (lightface lines: O6 + CS model solid, VIP4 + CS model dashed) and plasma frequency (boldface line: ionosphere + Bagenal torus model with $T_\perp/T_{||} = 1$) versus distance from Jupiter's centre, along the $6\,R_J$ field line in the northern hemisphere, at a longitude of 112° (intersection of centrifugal and magnetic equators). Identical curves are obtained in the southern hemisphere, and marginally different ones at other longitudes and for $T_\perp/T_{||} = 2$. The grey-shaded region reflects the estimated error deduced from comparison with Galileo's measurements ($\times 0.5$ to $\times 2$ on the electron density). (b) Corresponding variation of $\varepsilon = (f_{pe}/f_{ce})^2$ computed with the O6 + CS and ionosphere + Bagenal models. Domains of $\varepsilon \geqslant 0.15$ and $0.02 \leqslant \varepsilon \leqslant 0.15$ are indicated (resp. in dark and light grey shading).

5. Analysis

5.1. Method

Fig. 4a displays the variations of the local gyrofrequency (lightface lines) and plasma frequency (boldface line) versus distance to the centre of Jupiter, along the $6\,R_J$ field line in the northern hemisphere, at a longitude of 112° (or

equivalently $112^\circ + 180^\circ$) where the centrifugal and magnetic equators cross and thus where the Io torus is symmetrical with respect to the magnetic equator. It illustrates the fact that $f_{ce} > f_{pe}$ within $\sim 5\ R_J$ while f_{pe} dominates beyond $\sim 5\ R_J$, which corresponds to the inner limit of Io's plasma torus.

Gyrofrequencies computed using the O6 model (solid line) and the VIP4 model (dashed line)—both including the same current sheet contribution—slightly differ very close to the planet, where the different high order multipolar terms of the two magnetic field models have a significant contribution. But, in the region we are interested in ($\sim 4\ R_J$) they are almost identical, so we will only use hereafter the O6 model with the current sheet (noted "O6 + CS"). Also, as we will further discuss in the final remarks below (Section 6.4), the results we obtain for the northern and southern hemispheres differ by less than 5%, and their variation with the longitude is approximately sinusoidal and remains within $\pm 10\%$ of that for the longitude 112°. So, although we have made calculations for both hemispheres and several longitudes, we will display results only for the northern hemisphere and a longitude of 112°, with the exception of those specifically concerning Io-DAM because Io-controlled arcs are known to mainly occur in a different range of longitudes (see Section 5.3).

The ionospheric contribution to the plasma frequency is limited to distances $\leqslant 1.1\ R_J$, so that details of the ionospheric model are unimportant. Beyond $\sim 1.1\ R_J$, the plasma distribution is that of Bagenal (1994), based on Voyager measurements, without any proton temperature anisotropy. The shaded region reflects the "worst case" error of a factor 2 inferred from the comparison of Voyager and Galileo measurements (as discussed in Section 4). Introducing a moderate thermal anisotropy of the hot ions ($T_\perp/T_{||} = 2$) slightly increases the equatorial confinement of the torus and results in a $\leqslant 5\%$ increase of the distance at which $f_{ce} \approx f_{pe}$ (and a similar decrease of the corresponding frequency), but as this parameter is poorly constrained by the observations, we will restrict below to results obtained with $T_\perp/T_{||} = 1$.

Fig. 4b displays the corresponding variation of $\varepsilon = (f_{pe}/f_{ce})^2$ computed with the O6 + CS magnetic field model and the ionosphere + Bagenal plasma model (at 112° longitude). Domains of $\varepsilon \geqslant 0.15$ and $0.02 \leqslant \varepsilon \leqslant 0.15$ are indicated (resp. in dark and light grey shading).

Fig. 5 is a different display of the same information, which allows us to test our hypothesis that the LF limit of Jovian radio components corresponds to ε reaching the critical value ε_{max} along their source field lines. Fig. 5a and b display the variations of the gyrofrequency versus the plasma frequency along field lines with apex at resp. 6 and $9\ R_J$. Io's torus corresponds to the lower part of each diagram and Jupiter's ionosphere to the upper part. Again, shaded areas are domains where $\varepsilon = \geqslant 0.15$ (dark grey), $0.02 \leqslant \varepsilon \leqslant 0.15$ (light grey), and $\varepsilon \leqslant 0.02$ (white). Cyclotron-maser radio emission is possible in the white area, and is quenched somewhere in the light grey area.

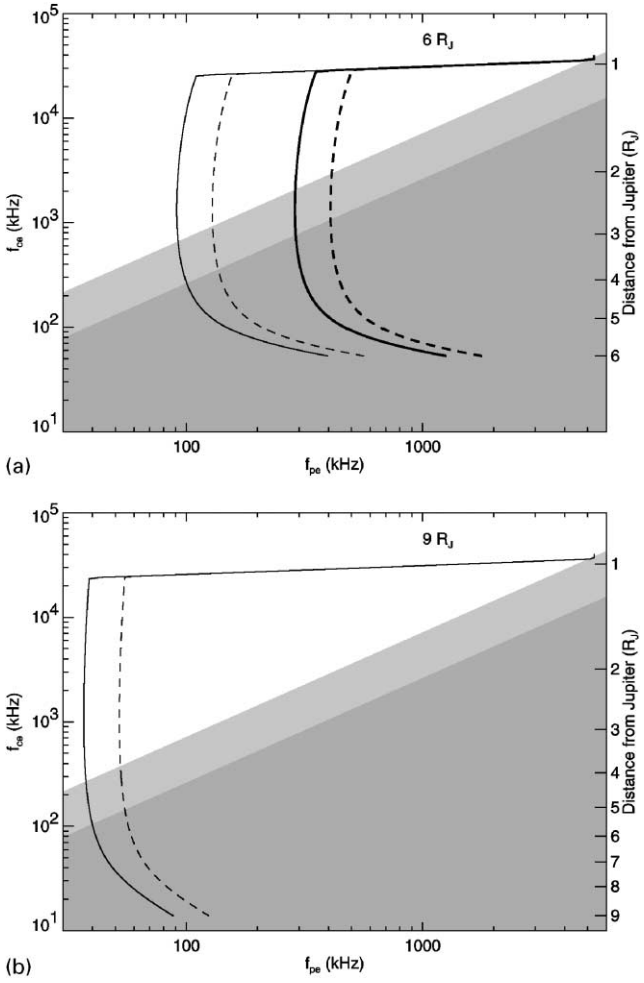

Fig. 5. (a) Gyrofrequency versus plasma frequency along the O6 + CS field line with apex at $6\ R_J$, in the northern hemisphere, for a longitude of 112°. Shaded areas correspond to $\varepsilon \geqslant 0.15$ (dark), $0.02 \leqslant \varepsilon \leqslant 0.15$ (light), and $\varepsilon \leqslant 0.02$ (white). The quasi-horizontal line at the top models Jupiter's ionosphere. The 4 curves correspond to the Bagenal model $\times 1$ (lightface solid), $\times 2$ (lightface dashed), $\times 10$ (boldface solid), and $\times 20$ (boldface dashed). CMI efficiency is quenched somewhere in the light-shaded area. (b) Same as (a) for the $9\ R_J$ field line and $\times 1$ and $\times 2$ scaling factors only.

Again, as justified above, all curves have been computed with the O6 + CS magnetic field model, in the northern hemisphere at a longitude of 112°, without any thermal ion anisotropy.

Lightface solid lines in Fig. 5a and b correspond to the Bagenal plasma model. Their intersections with the grey-shaded borders show that the CMI efficiency is quenched for a gyrofrequency between $\sim$ 260 and $\sim$ 650 kHz along the $6\ R_J$ field line, and between $\sim$ 100 and $\sim$ 260 kHz along the $9\ R_J$ field line. Use of a denser ($\times 2$) Bagenal model (lightface dashed lines) upshifts these four values by a factor $\approx \sqrt{2}$. Along the $6\ R_J$ field line only, Io's dense wake can be taken into account, as a first approximation, through a $\times 10$ to $\times 20$ factor applied to the

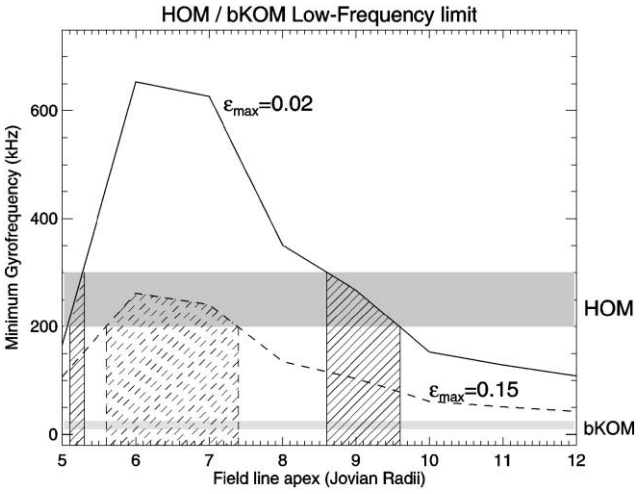

Fig. 6. Minimum gyrofrequency that can be generated through CMI versus field line apex (O6 + CS model, northern hemisphere, longitude = 112°), for $\varepsilon_{max} = 0.02$ (solid line) and $\varepsilon_{max} = 0.15$ (dashed line). Shaded regions correspond to observed HOM and bKOM LF limits. The hatched areas identify domains where the minimum gyrofrequency corresponding to CMI-quenching matches the observed HOM LF limit (200–300 kHz).

Bagenal model (boldface lines on Fig. 5a), and leads to a CMI-quenching range of 0.7–3 MHz.

5.2. HOM and bKOM low-frequency limits and source locations

Fig. 6 gathers results such as those of Fig. 5 for field lines with apex at 5–12 R_J. The minimum gyrofrequency corresponding to CMI quenching is plotted versus field line apex for $\varepsilon_{max} = 0.02$ (solid line) and $\varepsilon_{max} = 0.15$ (dashed line), using the Bagenal model. The shaded regions correspond to observed HOM and bKOM LF limits. The hatched areas identify domains where the minimum gyrofrequency that can be generated through CMI matches the observed HOM LF limit, i.e., 250 ± 50 kHz (cf. Section 2.2). The condition $\varepsilon_{max} = 0.15$ would imply that HOM emission is produced along field lines with apex between 5.6 and 7.4 R_J, while $\varepsilon_{max} = 0.02$ gives source regions along 5.1–5.3 R_J and/or 8.6–9.6 R_J field lines. In any case, HOM cannot originate from field lines with apex $< 5.1\ R_J$ or $> 9.6\ R_J$ because in that case, it should reach frequencies significantly lower than 200 kHz (e.g., ∼ 40–110 kHz along 12 R_J field lines).

As mentioned above, hot ions thermal anisotropy up to $T_\perp/T_{||} = 2$ modifies the above figures by less than 5%, and at longitudes $\neq 112^\circ$ (and $\neq 112^\circ + 180^\circ$) the symmetry between the northern and southern hemisphere breaks, as the magnetospheric plasma distribution centered around the centrifugal equator is no more symmetrical with respect to the magnetic equator, resulting in a ±10% variation of CMI-quenching gyrofrequencies around the above values.

In the case of bKOM, Fig. 6 also shows that a LF limit of 10–20 kHz (light-shaded region) corresponds to CMI quenching along field lines with apex well beyond 12 R_J.

5.3. Low-frequency limit and source location of Io-controlled emission

Fig. 6 shows that the observed LF limit of Io-controlled DAM between 1 and 2 MHz cannot be explained by CMI quenching in the frame of the Bagenal model of Iogenic magnetospheric plasma. Even with $\varepsilon_{max} = 0.02$, and the most "optimistic" interpretation of Galileo's measurements (×2 scaling factor applied to the Bagenal model), the highest LF limit derived along the 6 R_J field line is ⩽650 kHz (at 112°, with ±10° longitudinal variations).

However, as explained in Section 4, Galileo radio occultation measurements have revealed a dense plasma wake past Io, 10–20 times denser than the average torus. As a first rough approximation, we can model the total electron density along field lines crossing the wake with an upscaled Bagenal model (with a scaling factor up to ×20 applied to equatorial densities prior to computing the diffusive equilibrium along field lines). Fig. 7a illustrates the effect of this modelling on the LF limit of cyclotron-maser radio emission produced along the 6 R_J field lines crossing Io's wake. The minimum gyrofrequency corresponding to CMI quenching is plotted there versus the scaling factor (×1 to ×20) applied to the Bagenal model. It is found to lie in the range ∼ 0.8–2.2 MHz for a factor ×10, and in the range ∼ 1.2–3.1 MHz for a factor ×20. These ranges are consistent with the observed one for the Io-DAM LF limit (shaded).

As a more elaborate second step, we used the wake composition and temperature estimated by Frank et al. (1996) as inputs to the diffusive equilibrium. With Te ∼ 2 eV and Ti ∼ 11 eV, the wake appears colder than the rest of the torus (Te ∼ 5 eV, Ti ∼ 100 eV). Close examination of the Bagenal model shows that protons (with a number concentration ∼ 3.5% and a temperature of 60 eV), and to a lesser extent suprathermal heavy ions (with total concentration ∼ 15% and temperature ∼ 200 eV) provide a major contribution to the vertical scale height of the torus, and thus control the minimum CMI-quenching gyrofrequency. Although Frank et al. (1996) did not provide any constraint on protons or suprathermal ions in the wake, at least the former should be present due to the effect of photoionization or charge exchange processes on the atomic hydrogen in Io's atmosphere (see e.g., Frank and Paterson, 1999). We have thus tested the addition to the thermal ion population measured by Frank et al. of a 0–5% relative proton concentration with temperature in the range 10–60 eV, before running the diffusive equilibrium along field lines. Our results are summarized in Fig. 7b, where the minimum gyrofrequency corresponding to CMI quenching is plotted versus the proton concentration for several proton temperatures. It appears clearly that the

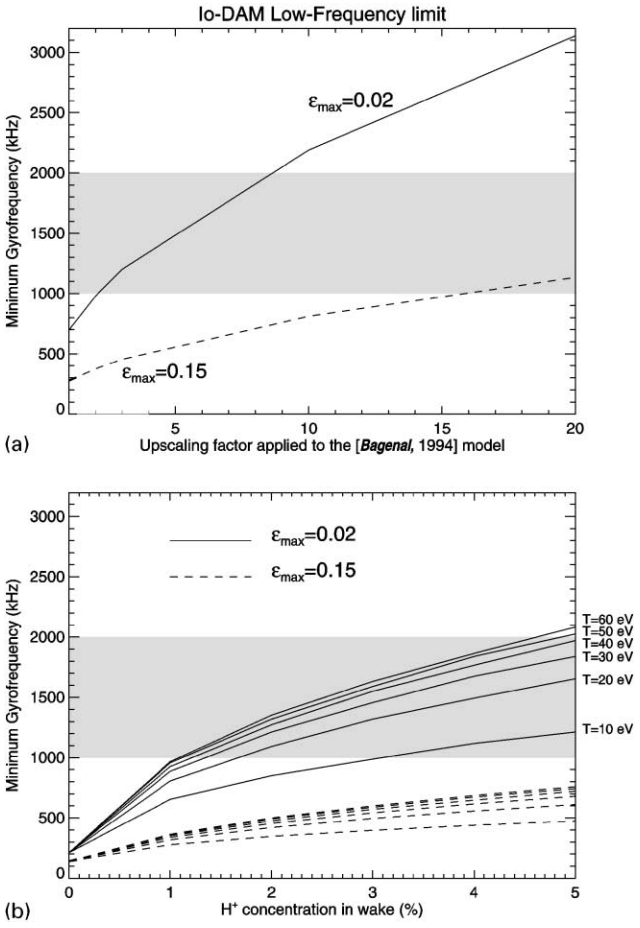

Fig. 7. (a) Minimum gyrofrequency that can be generated through CMI versus the upscaling factor of the Bagenal model ($\times 1$ to $\times 20$) accounting for the dense plasma in Io's wake, along the 6 R_J field line (O6 + CS model, northern hemisphere, longitude = 230° = average longitude of Io when Io-DAM radio emission is detected). The shaded region corresponds to observed Io-DAM LF limit. The curve for $\varepsilon_{max} = 0.15$ (dashed) is marginally consistent with observed LF limits, and requires a scaling factor > 16. (b) Minimum gyrofrequencies that can be generated through CMI versus relative proton concentration in the wake (added to the wake composition measured by Galileo), for several proton temperatures. The condition $\varepsilon_{max} = 0.15$ (dashed) cannot be reconciled with observed LF limits.

observed LF limit of Io-DAM (shaded) is incompatible with the condition $\varepsilon_{max} = 0.15$ (dashed lines). For $\varepsilon_{max} = 0.02$, a LF limit between 1 and 2 MHz is found for $n_{H+} > 1\%$ and $T_{H+} \geqslant 20$ eV (or even $T_{H+} \geqslant 10$ eV if $n_{H+} \geqslant 3\%$). As a comparison, Chust et al. (1999) derived from plasma wave analysis an iogenic hydrogen concentration $\geqslant 0.5\%$ at ~ 2 Io radii from the surface.

Note that, contrary to the previous figures Fig. 7a and b are plotted for a longitude of 230°. This is because Io-controlled emission (Io-DAM "arcs") is detected only when Io's longitude is in the range $\sim 150°$ to $\sim 300°$ (see Fig. 7a of (Genova and Aubier, 1985); and Fig. 6 of (Queinnec and Zarka, 1998)). We have thus taken 230° as a typical average source longitude for Io-DAM, preferably to the longitude of 112° chosen in the case of Io-independent emissions (as HOM and bKOM). Note that our results are weakly dependent on this longitude (of 230°) and are basically unchanged by any choice in the range $\sim 230 \pm 30°$.

In summary, the LF limit of Io-controlled radio emissions about 1–2 MHz is consistent with a source location along the 6 R_J Jovian field lines intersecting Io's plasma wake where it is ~ 2–10 times denser than the average torus, and suggests a concentration > 1–3% of hydrogen ions in this wake, depending on their temperature (Fig. 7b).

The longitudinal extent of the wake could not be directly deduced from Galileo observations, as the spacecraft flew within 700 km of Io through the wake. It has been estimated from theoretical considerations about the wake reacceleration to be in the range 0.75–5.5 R_J (i.e., 7°–53° in longitude), depending on Jupiter's conductance, not including the wake lengthening due to the added inertia of fresh plasma from Io (Crary and Bagenal, 1997). Another indication comes from the frequent occurrence of the HOM attenuation band (Gurnett et al., 1998) supporting an extended wake. This extent may be related to that of the UV trail of Io's footprint ($\sim 90°$ along Io's L-shell) revealed by Hubble Space Telescope (HST/STIS) images.

6. Discussion

6.1. Location of Jovian radio sources

We have thus demonstrated that the LF limits of Jovian Io-DAM (or more precisely of Io's control on Jovian radio emissions, i.e., 1–2 MHz) and of HOM emission (200–300 kHz) can be both attributed to the quenching of their common generation mechanism (the CMI) where the ratio f_{pe}/f_{ce} reaches a critical value along their source field lines. From results on Io-DAM obtained in the previous section, the relevant critical value appears to be $\varepsilon_{max} \approx 0.02$, i.e., $(f_{pe}/f_{ce})_{max} \approx 0.14$. This occurs in Io's plasma torus for the HOM component, and in Io's dense plasma wake for the Io-DAM. As a consequence, we infer new constraints on Jovian radio source locations: Io-DAM is found to extend along the 6 R_J field lines intersecting Io's wake (where the electron density is ~ 2–10 times higher than in the average torus), while HOM sources should lie along magnetic field lines with apex at 5–10 R_J, but not intersecting Io's wake. The range of possible HOM source locations can be restricted further if one considers, by analogy with the case of Io-DAM, that only the condition $\varepsilon_{max} \approx 0.02$ should be taken into account. In that case, field lines with apex between 5.3 and 8.6 R_J lead to a minimum CMI-quenching gyrofrequency > 300 kHz, inconsistent with observations, and must then be excluded (Fig. 6). Moreover, the strong solar wind control of HOM (Zarka and Genova, 1983) tends to favour more external field lines, with higher apex, for its source location (although the density gradients that seem to exist near 5 R_J (Bagenal et al., 1997) may cause particle acceleration there). We are thus left with a range of equatorial

distances $\sim$ 8.6–9.6 R_J for the best candidate HOM source field lines. Taking into account maximum overall variations of about $\pm$15%, versus longitude and hemisphere, this interval broadens to the range $\sim$ 7 to 11 R_J.

For bKOM, the LF limit of 10–20 kHz and the condition $\varepsilon_{max} \approx 0.02$ imply source field lines with apex distance $\gg 12\ R_J$.

As a comparison, Ulysses-URAP direction-finding results, for the few examples of slowly varying emissions for which the procedure could be applied with confidence, give—in the frame of the D4 model of Smith et al. (1976)—HOM sources in the $L = 7$–11 range, and bKOM sources between $L = 9$ and 15 (Ladreiter et al., 1994). As explained in the appendix (Fig. 9b and c), the range $L = 7$–11 in the D4 model at HOM frequencies ($\sim$ 300 kHz–1 MHz) corresponds to field lines with apex between 7 and $> 30\ R_J$ in the O6 + CS model. Our above results allow thus to restrict this range to 7–11 R_J only (or $L = 7$–9), i.e., to field lines crossing the external part of the Io torus (and in addition, the radial source extent in any limited longitude sector is probably smaller than that overall range).

The source of the precipitated electrons required for radio emission generation could be pitch angle scattering of electrons by VLF waves. VLF noise ($\leqslant$10 kHz) was indeed detected on $L = 7$–9 field lines at a longitude $\approx 100^\circ$, when Ulysses traversed Io's torus on February 8, 1992 (Farrell et al., 1993; Rézeau et al., 1997). Although a physical association with HOM is not demonstrated, both phenomena appear to originate on the same field lines and require electrons with keV energy. If the physical association is confirmed, this could make HOM the first radio emission clearly associated with diffuse aurora. No such component is known in the Terrestrial magnetosphere.

Conversely for bKOM, $L = 9$–15 at 100–300 kHz in the D4 model corresponds to field lines with apex $> 10\ R_J$ (up to open field lines—cf. Fig. 9a and b). Our analysis, implying an apex distance $\gg 12\ R_J$ (Fig. 6), favours field lines connected to distant parts of Jupiter's (middle to external) magnetosphere, or opened to the solar wind.

A Jovian UV auroral arc, made of fluctuating bright UV spots, was detected at $L \approx 15$ by HST's faint object camera a few hours after Ulysses' closest approach to Jupiter (Dols et al., 1992), which could well be associated to bKOM. In the same period, Ulysses detected in situ, at $\sim 20\ R_J$ from Jupiter, field-aligned currents which were mapped to auroral field lines $L = 12$–15 (Dougherty et al., 1993; Gérard et al., 1993). If a physical association was confirmed, then bKOM would appear as the true Jovian counterpart of AKR.

In light of our results (complementing Ulysses-URAP direction-finding ones), the main physical difference between HOM and bKOM now appears to be their clearly distinct source field lines, and hence the origin of the underlying accelerated electrons, rather than their emitted frequency range, which may occasionally overlap. Due to their beaming at large angle from the local magnetic field and refraction by the torus (see Zarka, 1998; and references therein), HOM and bKOM are detected in different—but overlapping—frequency ranges and at different CML by a near-equatorial observer (e.g., Lecacheux et al., 1992). But, when leaving Jupiter at high southern latitudes, Ulysses-URAP detected instead an unique sporadic emission similar to bKOM in a frequency range intermediate between those of HOM and bKOM.

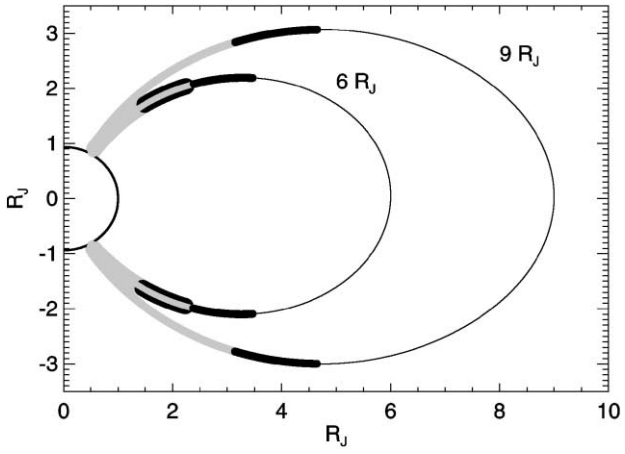

Fig. 8. Jovian radio source extents along the 6 and 9 R_J field lines (O6 + CS model, both hemispheres, longitude = 112°). Light-grey narrow bars represent regions where $\varepsilon \leqslant 0.02$, and black narrow bars regions where $0.02 \leqslant \varepsilon \leqslant 0.15$, using the Bagenal model of the Io torus. Thick bars along the 6 R_J field line represent similar ranges of ε along field lines intersecting Io's wake, modeled by a upscaled ($\times$10) Bagenal model.

Although we have listed in the Section 1 arguments in favour of HOM being the LF extent of Io-independent DAM (spectrum continuity, correlation of occurrence), similar and additional arguments do exist in favour of bKOM being actually this LF extent, as the correlations found between UV aurora and Io-independent DAM (Prangé et al., 1993a, b). Definitive answer to this question will require a statistical study of occurrence and frequency ranges of these three radio components, preferably observed from several vantage points (e.g., using Galileo, Cassini...), and the modelling of these observations taking into account the emissions' beaming as well as propagation (refraction) effects.

6.2. Source extent

Our above analysis of CMI quenching as a function of ε also constrains the radio source extents along Jovian field lines. For example, field lines with apex at 6 and 9 R_J are displayed on Fig. 8. In the frame of the Bagenal model, regions where $\varepsilon \leqslant 0.02$ (light-grey narrow bars), and where $0.02 \leqslant \varepsilon \leqslant 0.15$ (black narrow bars) are superimposed on O6 + CS field lines at a longitude of 112°. Along the 6 R_J field line, the same regions are also represented (thick bars) in the frame of an upscaled ($\times$10) Bagenal model (as explained in Section 5.3, a longitude about 230° is more relevant for the case of Io-DAM, but this does not affect significantly the sketch of Fig. 8). The Io-DAM LF cutoff strongly suggests that the relevant condition for

CMI-quenching is $\varepsilon_{max} = 0.02$, as observed at the Earth in AKR source regions (Hilgers, 1992, 1995).

Limitations on source extent imposed by CMI-quenching appear quite effective, limiting the radio source extent to an altitude $\leqslant 3 \pm 0.5\, R_J$ along the $6\, R_J$ field line ($\leqslant 2\, R_J$ for field lines intersecting Io's wake), and $\leqslant 4 \pm 1\, R_J$ along the $9\, R_J$ field line.

Due to the absence of any equivalent to the Io torus, these limitations do not apply in other planetary magnetospheres, but are replaced by much weaker constraints, such as the vertical extent of the equatorial current sheet or magnetodisc at Saturn (Zarka, 1992b). At Uranus and Neptune, the large dipole tilt on the rotation axis tends to deplete equatorial regions, from which X mode radio emissions have thus been detected by the Voyager radioastronomy experiment (see Zarka, 1998, and references therein). At Earth, the effect of the plasmasphere on CMI-quenching is unclear but probably marginal as (i) its boundary is tangent to magnetic field lines (rather getting across them like Io's torus), and (ii) AKR is emitted along magnetic field lines at significantly higher latitudes than the plasmasphere boundary.

6.3. Proton concentration in Io's wake

From Section 5.3 it appears that the Io-DAM LF cutoff can help to constrain the proton concentration in Io's plasma wake. In order for the LF cutoff computed through diffusive equilibrium to match the observed one, a concentration $n_{H+} > 1\%$ (and temperature $T_{H+} \geqslant 20$ eV if $n_{H+} < 3\%$—cf. Fig. 7b) is required in addition to the composition measured by Frank et al. (1996). As a consequence, monitoring of the LF cutoff of Io's control on Jovian radio emissions in the range 0–3 MHz could reveal time variations of this proton concentration in the wake.

6.4. Final remarks

A complete parametric study of the CMI-quenching condition has been performed versus field line apex, plasma anisotropy $T_\perp/T_{||}$, and scaling factor (relative to the Bagenal model), for several Jovian longitude and both hemispheres, and for two magnetic field models (O6 + CS & VIP4 + CS). As already mentioned above, we have found that:

- the choice of the internal magnetic field model is unimportant because they are identical at the distance at which ε reaches any of its critical values;
- results for the northern and southern hemispheres differ by $\leqslant 5\%$;
- results for different longitudes vary within $\pm 10\%$ around that for the longitude 112° (or equivalently $112^\circ + 180^\circ$), for which the Io torus is at the magnetic equator;
- the thermal anisotropy of the hot ions, poorly constrained by the observations, has a weak impact ($\leqslant 5\%$) on the results.

For a given field line apex and value of ε_{max}, the cumulated effects of all the above parameters induce variations of 10–20% amplitude. These variations are smaller than the effect of the choice of ε_{max} (0.02 or 0.15), and of the same order of magnitude than the uncertainty which affects the determination of the instantaneous LF limit of any radio component (and in addition, we have no information on the possible existence of small-scale filamentary cavities in Jovian auroral regions, possibly similar to AKR sources (Hilgers, 1992)). Thus, we have chosen for clarity to display in Fig. 4–8 only those results obtained with the O6 + CS model, in the northern hemisphere (both hemispheres for the sketch of Fig. 8), at a longitude of 112° (230° in Fig. 7), and for $T_\perp/T_{||} = 1$ (no thermal anisotropy). The longitude of 112° (or $112^\circ + 180^\circ$) is the one around which fluctuations for other longitudes are symmetrical, and is thus the best choice for Io-independent emissions (HOM, bKOM), for which the source longitude is not strongly constrained. Conversely, as discussed in Section 5.3, a longitude about 230° is better adapted to the case of Io-controlled emission ("Io-DAM").

In spite of the limitations linked to the value of ε_{max} and to the difficulty of measuring precisely LF limits, we think that we fairly understand now the origin of the frequency ranges covered by the various Jovian radio components, so that it becomes possible to use them for remotely sensing the Jovian environment.

Acknowledgements

We thank Hubert de Lassus for computer recognition of nKOM and Solar type III bursts in the Ulysses-URAP data (Section 2), Fran Bagenal for her help in the modelling of the plasma density in Io's torus and wake (Sections 4 and 5.3), and Renée Prangé for her comments on the limitations of the "L-shell" concept and her suggestion to include a comparison of magnetic field models (Appendix). The Ulysses URAP experiment is a joint project of NASA/GSFC, the Observatoire de Paris, CRPE, and University of Minnesota. The French contribution was supported by the CNES and the CNRS.

Appendix A. Comparison of D4 and O6 (+CS) model field lines

The D4 model (Smith et al., 1976) is the best fit of an offset tilted dipole with Pioneer magnetometer measurements close to Jupiter. The O6 model of Jupiter's internal field was derived from the generalized inversion of magnetometer measurements from Pioneer and Voyager flybys (Connerney, 1992). The concept of L-shell being unambiguous—and even meaningful—only in a dipolar field, and the D4 model being little different from the O6 one above $\sim$ 2–3

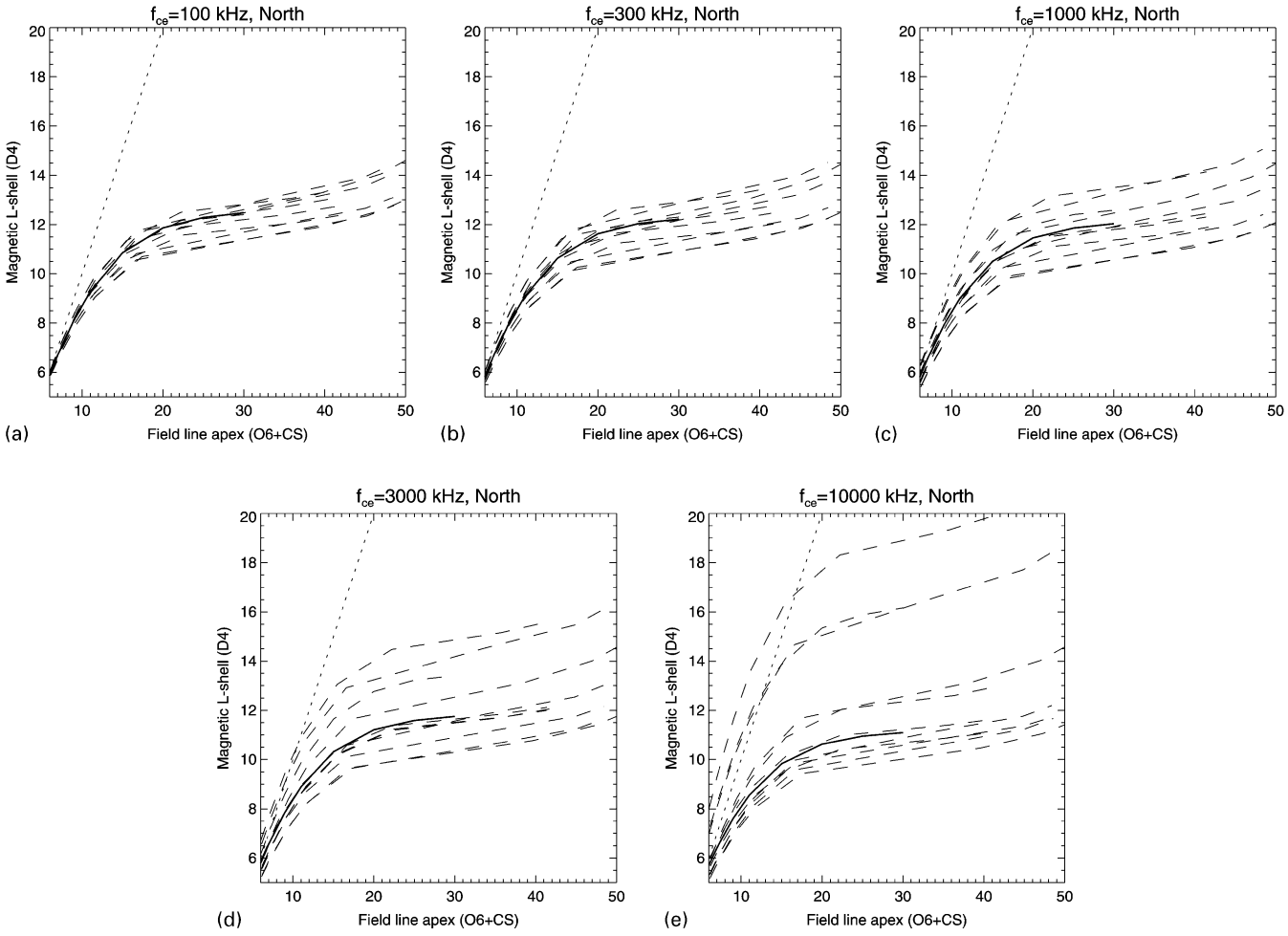

Fig. 9. (a) L-shell of D4 magnetic field lines crossing O6 + CS field lines (characterized by their apex distance) at the altitude where the local gyrofrequency is $f_{ce} = 100$ kHz, in the northern hemisphere. L values and apex distances are in Jovian radii (R_J). The solid line correspond to 112° longitude, and the dashed lines to longitudes $112^\circ + n \times 30^\circ (n = 1, 11)$. The dotted line is the bisector (L = apex distance). (b)–(e) same as a, for $f_{ce} = 300$, 1000, 3000 and 10 000 kHz.

R_J altitude at high magnetic latitudes, the D4 model was largely used to characterize HOM and bKOM source field lines as a result of radio direction-finding studies (see e.g., Ladreiter et al., 1994; Reiner et al., 1993a). However, the Jovian current sheet (or magnetodisc) (Connerney et al., 1981) stretches field lines at low magnetic latitudes beyond $\sim$ 5–10 R_J, and its contribution must be taken into account when looking at the true apex of a given field line, and for example at its consequences in terms of the origin of accelerated electrons.

In this paper, we have used the O6 model + current sheet (O6 + CS) in the computations. We have checked that the results are identical to those obtained with the VIP4 + CS model (cf. Fig. 4a). However, in the discussion, comparison of our results to earlier ones requires a detailed comparison of D4 and O6 + CS field lines, which is function of the frequency.

Fig. 9a–e thus display D4 magnetic L-shells versus the apex of more realistic field lines computed with the O6 + CS model for longitudes of 112° (solid lines) and $112^\circ + n \times 30^\circ$ ($n = 1, 11$—dashed lines). The corresponding D4 L-shells have been determined at 5 gyrofrequencies along each field line, and plotted versus the apex distance of the O6 + CS field lines. It appears clearly that D4 L-shells are generally smaller than the O6 + CS apex (as expected), and that the value of L increases with decreasing gyrofrequency, which reflects the field line stretching by the current sheet.

For example, for HOM sources, the range $L = 7$–11 was derived in the frame of the D4 model by Ladreiter et al. (1994) for frequencies between $\sim$ 300 kHz and 1 MHz. Fig. 9b and c show that this range translates into field line apex between 7 and $> 30\,R_J$ in the frame of the O6 + CS model. Fig. 9 may of course be used for the reverse conversion from O6 + CS to D4.

References

Alexander, J.K., Carr, T.D., Thieman, J.R., Schauble, J.J., Riddle, A.C., 1981. Synoptic observations of Jupiter's radio emissions: average statistical properties observed by Voyager. J. Geophys. Res. 86, 8529–8545.

Bagenal, F., 1994. Empirical model of the Io plasma torus: Voyager measurements. J. Geophys. Res. 99, 11,043–11,062.

Bagenal, F., Crary, F.J., Stewart, A.I.F., Schneider, N.M., Gurnett, D.A., Kurth, W.S., Frank, L.A., Paterson, W.R., 1997. Galileo measurements of plasma density in the Io torus. Geophys. Res. Lett. 24, 2119–2122.

Benson, R.F., 1995. Comment on "The auroral radiating plasma cavities" by A. Hilgers. Geophys. Res. Lett. 22, 3005–3007.

Bigg, E.K., 1964. Influence of the satellite Io on Jupiter's decametric emission. Nature 203, 1008–1010.

Boischot, A., Lecacheux, A., Kaiser, M.L., Desch, M.D., Alexander, J.K., Warwick, J.W., 1981. Radio Jupiter after Voyager: an overview of the Planetary Radio Astronomy observations. J. Geophys. Res. 86, 8213–8226.

Burke, B.F., Franklin, K.L., 1955. Observations of a variable radio source associated with the planet Jupiter. J. Geophys. Res. 60, 213–217.

Carr, T.D., Desch, M.D., Alexander, J.K., 1983. Phenomenology of magnetospheric radio emissions. In: Dessler, A.J. (Ed.), Physics of the Jovian Magnetosphere. Cambridge University Press, New York, pp. 226–284.

Chust, T., Roux, A., Perraut, S., Louarn, P., Kurth, W.S., Gurnett, D.A., 1999. Galileo plasma wave observations of iogenic hydrogen. Planet Space Sci. 47, 1377–1387.

Connerney, J.E.P., 1992. Doing more with Jupiter's magnetic field. In: Rucker, H.O., Bauer, S.J., Kaiser, M.L. (Eds.), Planetary Radio Emissions III. Austrian Academic Science Press, Vienna, pp. 13–33.

Connerney, J.E.P., Acuña, M.H., Ness, N.F., 1981. Modeling the Jovian current sheet and inner magnetosphere. J. Geophys. Res. 86, 8370–8384.

Connerney, J.E.P., Acuña, M.H., Ness, N.F., Satoh, T., 1998. New models of Jupiter's magnetic field constrained by the Io flux tube footprint. J. Geophys. Res. 103, 11,929–11,939.

Crary, F.J., 1998. Io's interaction with the Jovian magnetosphere: Models of particle acceleration and scattering, Ph.D. Thesis, University of Colorado, Boulder.

Crary, F.J., Bagenal, F., 1997. Coupling the plasma interaction at Io to Jupiter. Geophys. Res. Lett. 24, 2135–2138.

Crary, F.J., Bagenal, F., Frank, L.A., Paterson, W.R., 1998. Galileo plasma spectrometer measurements of composition and temperature in the Io plasma torus. J. Geophys. Res. 103, 29,359–29,370.

de Lassus, H., Lecacheux, A., 1997. Automatic recognition of low-frequency radio planetary signals. In: Rucker, H.O., Bauer, S.J., Lecacheux, A. (Eds.), Planetary Radio Emissions IV. Austrian Academic Science Press, Vienna, pp. 359–368.

Desch, M.D., 1980. Io control of Jovian radio emission. Nature 287, 815–817.

Desch, M.D., Carr, T.D., 1978. Modulation of the Jovian emission below 8 MHz. Astron. J. 83, 828–837.

Dols, V., Gérard, J.C., Paresce, F., Prangé, R., Vidal-Madjar, A., 1992. Ultraviolet imaging of the Jovian aurora with the Hubble Space Telescope. Geophys. Res. Lett. 19, 1802–1806.

Dougherty, M.K., Southwood, D.J., Balogh, A., Smith, E.J., 1993. Field-aligned currents in the Jovian magnetosphere during the Ulysses flyby. Planet Space Sci. 41, 291–300.

Farrell, W.M., MacDowall, R.J., Hess, R.A., Kaiser, M.L., Desch, M.D., Stone, R.G., 1993. An interpretation of the broadband VLF waves near the Io torus as observed by Ulysses. J. Geophys. Res. 98, 21,177–21,188.

Frank, L.A., Paterson, W.R., Ackerson, K.L., Vasyliunas, V.M., Coroniti, F.V., Bolton, S.J., 1996. Plasma observations at Io with the Galileo spacecraft. Science 274, 394–395.

Frank, L.A., Paterson, W.R., 1999. Production of hydrogen ions at Io. J. Geophys. Res. 104, 10,345–10,354.

Genova, F., Aubier, M.G., 1985. Io-dependent sources of the Jovian decameter emission. Astron. Astrophys. 150, 139–150.

Genova, F., Zarka, P., Barrow, C.H., 1987. Voyager and Nanç ay observations of the Jovian radio emission at different frequencies: solar wind effect and source extent. Astron. Astrophys. 182, 159–162.

Genova, F., Zarka, P., Lecacheux, A., 1989. Jupiter decametric radiation. In: Belton, M.J.S., West, R.A., Rahe, J. (Eds.), Time-Variable Phenomena in the Jovian System, Vol. 494. NASA Spec. Publications, pp. 156–174.

Gérard, J.C., Dols, V., Paresce, F., Prangé, R., 1993. Morphology and temporal variations of the UV aurorae of Jupiter with HST. J. Geophys. Res. 98, 18,793–18,802.

Gurnett, D.A. et al, 2001. The Cassini Radio and Plasma Wave investigation. Space Sci. Rev., in press.

Gurnett, D.A., Kurth, W.S., Menietti, J.D., Persoon, A.M., 1998. An unusual rotationally modulated attenuation band in the Jovian hectometric radio emission spectrum. Geophys. Res. Lett. 25, 1841–1844.

Gurnett, D.A., Kurth, W.S., Roux, A., Bolton, S.J., Kennel, C.F., 1996. Galileo plasma wave observations in the Io plasma torus and near Io. Science 274, 391–392.

Hilgers, A., 1992. The auroral radiating plasma cavities. Geophys. Res. Lett. 19, 237–240.

Hilgers, A., 1995. Reply to the comment by R. F. Benson. Geophys. Res. Lett. 22, 3009–3010.

Hinson, D.P., Twicken, J.D., Karayel, E.T., 1998. Jupiter's ionosphere: new results from Voyager 2 radio occultation measurements. J. Geophys. Res. 103, 9505–9520.

Kaiser, M.L., Desch, M.D., 1992. Jovian broadband kilometric radiation: new observations from Ulysses. In: Rucker, H.O., et al. (Eds.), Planetary Radio Emissions III. Austrian Academic Science Press, Vienna, pp. 35–43.

Kaiser, M.L., Desch, M.D., Farrell, W.M., MacDowall, R.J., Stone, R.G., Lecacheux, A., Pedersen, B.M., Zarka, P., 1992. Ulysses Observations of Escaping VLF Emissions from Jupiter. Geophys. Res. Lett. 19, 649–652.

Kaiser, M.L., Garcia, L.N., 1997. Jupiter's low-frequency radio spectrum: filling in the gaps. In: Rucker, H.O., et al. (Eds.), Planetary Radio Emissions IV. Austrian Academic Science Press, Vienna, pp. 17–24.

Kurth, W.S., Bolton, S.J., Gurnett, D.A., Levin, S., 1997. A determination of the source of Jovian hectometric radiation via occultation by Ganymede. Geophys. Res. Lett. 24, 1171–1174.

Ladreiter, H.P., Leblanc, Y., 1989. Jovian hectometric radiation: beaming, source extension, and solar wind control. Astron. Astrophys. 329, 297–310.

Ladreiter, H.P., Leblanc, Y., 1991. The Jovian hectometric radiation: an overview after the Voyager mission. Ann. Geophys. 9, 784–796.

Ladreiter, H.P., Zarka, P., Lecacheux, A., 1994. Direction-finding study of Jovian hectometric and broadband kilometric radio emissions: evidence for their auroral origin. Planet Space Sci. 42, 919–931.

Lecacheux, A., Boudjada, M.Y., Rucker, H.O., Bougeret, J.L., Manning, R., Kaiser, M.L., 1998. Jovian decameter emissions observed by the Wind/WAVES radioastronomy experiment. Astron. Astrophys. 329, 776–784.

Lecacheux, A., Pedersen, B.M., Zarka, P., Aubier, M.G., Desch, M.D., Farrell, W.M., Kaiser, M.L., MacDowall, R.J., Stone, R.G., 1992. In ecliptic observations of Jovian radio emissions by Ulysses: comparison with Voyager results. Geophys. Res. Lett. 19, 1307–1310.

Le Quéau, D., Pellat, R., Roux, A., 1985. The Maser synchrotron instability in an inhomogeneous medium: application to the generation of auroral kilometric radiation. Ann. Geophys. 3, 273–292.

Louarn, P., 1992. Auroral planetary radio emissions: theoretical aspects. Adv. Space Res. 12 (8), 121–134.

Louarn, P., Perraut, S., Roux, A., Gurnett, D.A., Kurth, W.S., Bolton, S.J., 1997. The global plasma environment of Io as inferred from the Galileo plasma wave observations. Geophys. Res. Lett. 24, 2115–2118.

Menietti, J.D., Gurnett, D.A., Kurth, W.S., Groene, J.B., Granroth, L.J., 1998. Galileo direction finding of Jovian radio emissions. J. Geophys. Res. 103, 20,001–20,010.

Moncuquet, M., 1997. Équilibre et confinement du tore de plasma d'Io dans la magnétosphère de Jupiter: Observations d'Ulysse et modélisation, Thesis, Univ. Paris VII, Meudon, December.

Prangé, R., Shimmin, P., Zarka, P., 1993a. Des orages magnétiques sur Jupiter?. In: Hubert, D. (Ed.), Séminaire Scientifique Du Gdr Plasmae. Observ. de Paris, Meudon, pp. 56–60.

Prangé, R., Zarka, P., Ballester, G.E., Livengood, T.A., Denis, L., Carr, T.D., Reyes, F., Bame, S.J., Moos, H.W., 1993b. Correlated variations of UV and radio emissions during an outstanding jovian auroral event. J. Geophys. Res. 98, 18,779–18,791.

Queinnec, J., Zarka, P., 1998. Io-controlled decameter arcs and Io-jupiter interaction. J. Geophys. Res. 103, 26,649–26,666.

Reiner, M.J., Fainberg, J., Stone, R.G., 1993a. Source characteristics and locations of hectometric radio emissions from the northern Jovian hemisphere. Geophys. Res. Lett. 20, 321–324.

Reiner, M.J., Fainberg, J., Stone, R.G., Kaiser, M.L., Desch, M.D., Manning, R., Zarka, P., Pedersen, B.M., 1993b. Source characteristics of Jovian narrow-band kilometric radio emissions. J. Geophys. Res.-Planets 98, 13,163–13,176.

Rézeau, L., Cornilleau-Werhlin, N., Belmont, G., Canu, P., Prangé, R., Balogh, A., Forsyth, R.J., 1997. Possible role of electromagnetic low frequency waves in the Io torus in the production of Jovian aurorae. Planet Space Sci. 45, 483–493.

Smith, E.J., Davis Jr., L., Jones, D.E., 1976. Jupiter's magnetic field and magnetosphere. In: Gehrels, T. (Ed.), Jupiter. University of Arizona Press, Tucson, pp. 788–829.

Stone, R.G., et al., 1992. Ulysses radio and plasma wave observations in the Jupiter environment. Science 257, 1524–1531.

Warwick, J.W., Pearce, J.B., Peltzer, R.G., Riddle, A.C., 1977. Planetary Radio Astronomy experiment for the Voyager Missions. Space Sci. Rev. 21, 309–327.

Wu, C.S., Lee, L.C., 1979. A theory of terrestrial kilometric radiation. Astrophys. J. 230, 621–626.

Zarka, P., 1992a. The auroral radio emissions from planetary magnetospheres: what do we know, what don't we know, what do we learn from them? Adv. Space Res. 12(8), 99-(8)115.

Zarka, P., 1992b. Remote probing of auroral plasmas. In: Rucker, H.O., et al. (Eds.), Planetary Radio Emissions III. Austrian Academic Science Press, Vienna, pp. 351–369.

Zarka, P., 1998. Auroral radio emissions at the outer planets: observations and theories. J. Geophys. Res. 103, 20,159–20,194.

Zarka, P., Genova, F., 1983. Low frequency jovian emission and solar wind magnetic sector structure. Nature 306, 767–768.

Zarka, P., Prangé, R., 1994. The project "ORAJES": an earth orbiter for radio monitoring of Jupiter and Saturn, Bull. Am. Astr. Soc., (presented at the 25th Meeting of the Division of Planetary Sciences, AAS, 10/1993).